Explicit treatment of tensor force with a method of Antisymmetrized Molecular Dynamics

Akinobu DOTE[1], Yoshiko KANADA-EN'YO[2], Hisashi HORIUCHI[3], Yoshinori AKAISHI[4] and Kiyomi IKEDA[5]

[1]*High Energy Accelerator Research Organization (KEK), Ibaraki 305-0801, Japan*
[2]*Yukawa Institute for Theoretical Physics, Kyoto 606-8502, Japan*
[3]*Department of Physics, Kyoto University, Kyoto 606-8502, Japan*
[4]*College of Science and Technology, Nihon University, Funabashi 274-8501, Japan*
[5]*The Institute of Physical and Chemical Research (RIKEN), Saitama 351-0198, Japan*

In order to treat tensor force explicitly, we propose a microscopic model for nuclear structure based on antisymmetrized molecular dynamics (AMD). As a result of the present study, it is found that some extentions of the AMD method are effective to incorporate the tensor correlation into wave functions. Calculating the deuteron, triton and ^{4}He with the extended version of AMD, we obtained solutions that have large contribution of the tensor force. By analyzing the wave funtion of ^{4}He, it is found that its single-particle orbits are composed of normal-size $0s$ orbits and shrunk p orbits so as to gain the tensor force.

§1. Introduction

Tensor force plays important roles concerning various properties of nuclei. Recent studies with *ab initio* calculations show that the contribution of the tensor force to binding energies is large in $A \simeq 10$ light nuclei,[1)] as well as in few-nucleon systems.[2)] Besides the binding energies, effects of the tensor force on single-particle energies and nuclear structure have been suggested for a long time.[3),4)] Recently, several studies showed its influences on LS splitting,[5)] GT transitions and magnetic moments.[6)] These facts imply that direct effects of the tensor force may be revealed in some properties of nuclear structure.

The tensor force causes a characteristic correlation between two nucleons, which is called the *tensor correlation*. In the deuteron, the tensor force gives a large attraction due to the coupling of $^3S_1$ with $^3D_1$. Also, in ^{4}He, the $[JLS = 022]$ component is mixed to the dominant $(0s)^4$ component due to the tensor force. Since the tensor correlation between two nucleons is varied, depending on the environment surrounding them, the contribution of the tensor force is sensitive to the nuclear density and structure. According to analyses with the g matrix, as the density increases in nuclear matter, the contribution of the tensor force is suppressed (*tensor suppression*). This is a major cause of the nuclear saturation property.[7)] Reversely, as the density decreases, the tensor suppression becomes small. Therefore, the tensor force is considered to be important in light nuclei because they have a relatively large surface region, being low density. In Ref. [4], it is emphasized that the renormalization of the tensor force to an effective ^3E central force is very sensitive to the starting

energy as well as the density. Because the starting energy is strongly dependent on the structure of the total system, the tensor force gives a structure dependence to the effective interaction. Thus, the tensor force might be closely related to a variety of structures realized in light nuclei such as a clustering structure. Moreover, it is natural to expect that the tensor force may provide clarity to the problems of unstable nuclei, which usual approaches with effective nuclear forces sometimes fail to describe.

There are many kinds of model calculations that are useful for systematic studies of various nuclei in wide mass-number regions. They, however, have avoided any explicit treatment of the tensor force because of its difficulty. In such model calculations, one uses effective interactions that are either derived from realistic forces theoretically by renormalizing the tensor force into central and LS forces, or phenomenologically determined. In usual cases, the density dependence arising from the tensor force is simulated by phenomenological density-dependent or three-body forces. Such model calculations with effective interactions have succeeded to reproduce and explain many physical quantities of various nuclei. However, there remain some phenomena that those model calculations failed to reproduce without using system-dependent effective forces. The parity inversion problem of ^{11}Be and the binding mechanism of ^{11}Li are typical examples. Therefore, it is natural to expect that the effect of the tensor force might be a key to solve these problems.[8] Moreover, another drawback of the usual model calculations is that one can not discuss the effect of the tensor force on physical quantities in an explicit way, because the obtained wave functions do not contain a tensor correlation.

Our aim is to treat the tensor force as directly as possible in the model calculation. We would like to systematically investigate its contribution to the binding of various nuclei and the effects of the tensor correlation on the nuclear properties. We mention here a repulsive core of the nuclear force, which is another characteristic of a realistic nuclear force, and is not explicitly contained in the usual effective nuclear force as well as the tensor force. Recent developments in treating the repulsive core and the tensor force in a model calculation can be seen in the unitary correlator method,[9] the g-matrix method[10] and the V_{low-k} method.[11] Since the repulsive core should be less state-dependent than the tensor force, we consider that it can be smoothed out for the present purpose. We adopt an effective force where the repulsive core in the central force is smoothed by the g-matrix method in the present study.

To accomplish our purpose, we need a wave function that can contain the tensor correlation. We start from a mean-field approach, considering its applicability to wide mass-number regions. As already known, ordinary mean-field wave functions are insufficient to treat the tensor force. From the operator form of the tensor force, one can easily expect that two extensions are needed. The first one is i) *a parity-violating mean field and a strong correlation between spin and space.* The other point is ii) *flexibility of the isospin wave function.* The tensor force contains a parity-odd operator as a dominant term in a mean-field picture, and it also includes a charge-exchange term. Therefore, it is difficult to treat the tensor force within the usual mean-field approaches. In fact, the expectation value of the tensor operator vanishes

in a model space of a simple mean-field. The importance of the parity-violating mean field and charge mixing are already pointed out in the Ref. [12].

Several groups are currently challenging this theme. Sugimoto *et al.* are investigating the contribution of the tensor force in various nuclei, based on the relativistic[6] and non-relativistic[12] mean-field approaches. Myo *et al.* are investigating the effect of a tensor correlation in light unstable nuclei with an extended shell model.[5] We, here, adopt an antisymmetrized molecular dynamics (AMD) method[13] as a starting point of our model. Due to the simplicity of its framework, AMD can be easily improved, while corresponding to our requirements.[14–17] Since its wave function is simply composed of Gaussian wave packets, we can easily perform various projections, such as parity, angular momentum and charge number projections. The parity-violating mean field has already been realized by the parity projection in AMD. Other advantages of the AMD are that it does not rely on any model assumptions on nuclear structure, such as the existence of clusters and nuclear deformation, and that it is applicable to general nuclei over a wide mass-number region. It has succeeded to describe various structures and cluster aspects of light and middle nuclei.[13–17] We, therefore, expect that a model based on AMD can directly reveal a relation between the tensor force and various structures of light nuclei, including clustering structure, as investigated in Ref. [4]. On the other hand, in Refs.,[5,6,12] the model wave functions are based on mean-field approaches, and the single-particle orbits in ^{4}He are assumed to be linear combination of s and p-orbits. Based on the AMD method, we will see how the tensor correlation is realized in the wave functions without relying on such a model assumption.

In the present paper, we employ effective interactions that involve the tensor term explicitly, and extend the framework of AMD so that it can gain the contribution of the tensor force. We adopt an effective force that is derived from the Tamagaki potential[18] by smoothing the repulsive core of the central term, and also test another effective force: the Furutani-Tamagaki potential.[19] We calculate the deuteron, triton and ^{4}He with an extended version of AMD. We show the effects of i) *a parity-violating mean field and a strong correlation between spin and space* and ii) *the flexibility of the isospin wave function* in practical calculations. Moreover, we propose additional extensions of the AMD to gain the tensor force more effectively; iii) *linear combination of the wave packets that have different width parameters* and iv) *charge-, parity- and angular-momentum-projections*. Finally, we analyze the properties of the wave functions of the deuteron and ^{4}He obtained by the extended AMD, while focusing on the tensor correlation.

This paper is organized as follows. In section 2, we explain the extensions of the AMD framework. We investigate the effect of these extensions in the deuteron, triton and ^{4}He in section 3. Analysis of the obtained wave function of ^{4}He from the viewpoint of single particle levels is shown in section 4. In section 5, we give a summary and some discussions on further developments.

§2. Formalism

2.1. *Hamiltonian and tensor force*

The Hamiltonian used in this paper is

$$H = \sum_{i=1}^{A} t_i + \sum_{i<j=1}^{A} \left(v_{ij}^{C} + v_{ij}^{T} + v_{ij}^{Coulomb} \right) - T_{CM}. \tag{2·1}$$

Here, t_i is a kinetic energy term, $\frac{\boldsymbol{p}_i^2}{2m_N}$ ($\boldsymbol{p}_i$, momentum operator; m_N, nucleon mass); v_{ij}^{C}, v_{ij}^{T} and $v_{ij}^{Coulomb}$ indicate the central force, tensor force and Coulomb force, respectively. The center-of-mass motion energy, $T_{CM} = \frac{1}{2Am_N} \left(\sum_{i=1}^{A} \boldsymbol{p}_i \right)^2$, is removed. We employ two kinds of effective interactions, the Furutani-Tamagaki potential (F-T potential)[19] and the Akaishi(T) potential (AK(T) potential), as a set of v_{ij}^{C} and v_{ij}^{T}. Both potentials are described by a superposition of several range Gaussian wave packets:

$$v_{12}^{C} = \sum_{n=1}^{N} \left\{ C_n^{1E} P(^1E) + C_n^{3E} P(^3E) + C_n^{1O} P(^1O) + C_n^{3O} P(^3O) \right\} \exp\left[-(r/b_n)^2 \right], \tag{2·2}$$

$$v_{12}^{T} = \sum_{n=1}^{N} T_n^{3E} P(^3E)\ r^2 S_{12}\ \exp\left[-(r/b_n)^2 \right], \tag{2·3}$$

where $r = |\boldsymbol{r}_1 - \boldsymbol{r}_2|$. $N = 3$ in the F-T potential and $N = 10$ in the AK(T) potential. $P(X)$, $X = {}^1E$, ${}^3E$, ${}^1O$, ${}^3O$, is a projection operator and S_{12} is a tensor operator, $S_{12} = 3(\boldsymbol{\sigma}_1 \cdot \boldsymbol{r})(\boldsymbol{\sigma}_2 \cdot \boldsymbol{r})/r^2 - (\boldsymbol{\sigma}_1 \cdot \boldsymbol{\sigma}_2)$, where $\boldsymbol{r} = \boldsymbol{r}_1 - \boldsymbol{r}_2$. The radial part of the tensor force in both potentials is represented by a linear combination of $r^2\times$ Gaussians. The interaction parameters, $\{C_n^X, T_n^{3E}, b_n\}$, in the F-T potential are given in Ref. [19], and those in the AK(T) potential are given in Appendix. The Coulomb force, $v_{ij}^{Coulomb}$, is expressed by the superposition of seven range Gaussian wave packets.

The F-T potential was used in a cluster model study of ^{3}He+p scattering, and succeeded in reproducing scattering data, including polarization quantities and the spectra of ^{4}Li.[19] It can also reproduce the binding energy of ^{4}He with a harmonic-oscillator $(0s)^4$ wave function. The AK(T) potential is derived from the Tamagaki potential (OPEG),[18] which is a realistic nucleon-nucleon potential. The central part of the AK(T) potential is obtained by smoothing the repulsive core of the central part of OPEG with the method of g-matrix theory, whereas the tensor part remains to be the same as the original one of OPEG. In other words, the tensor force is not renormalized into the central one when constructing the AK(T) potential. The details of its derivation are explained in Ref. [10].*) The ${}^1E$ and ${}^3E$ central forces

*) In Ref. [10], the AV8' potential[21] is used and several values of the cut-off momentum, $k_Q^{(D)}$, for the tensor force are investigated. The AK(T) potential corresponds to the case that the Tamagaki potential is used instead of the AV8' potential and $k_Q^{(D)} = \infty$ fm^{-1}.

Fig. 1. (a) Furutani-Tamagaki potential and (b) Akaishi(T) potential. The ^1E and ^3E central potential and the ^3E tensor potential are shown as 'Central 1E', 'Central 3E' and 'Tensor 3E' in each panel, respectively. Both potentials are multiplied by r^2.

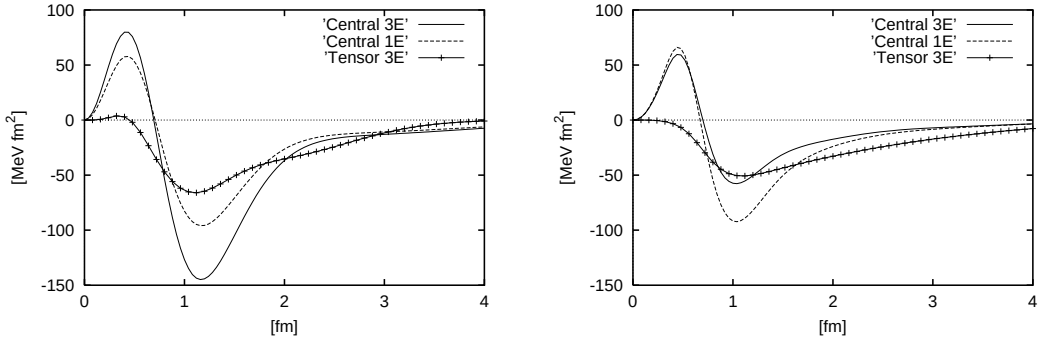

(a) Furutani-Tamagaki potential (b) Akaishi(T) potential

and the ^3E tensor force in both potentials are depicted in Figure 1. In the F-T potential, the ^3E central force is dominant, while the tensor force is smaller. On the other hand, the ^3E central force in the AK(T) potential is smaller than that in the F-T potential. The tensor force has almost the same magnitude as the ^3E central force in the AK(T) potential.

2.2. *Extended framework of AMD*

The details of the usual AMD framework are given in Refs. [13] and [20]. In order to incorporate the effect of the tensor force efficiently, we improve the single-nucleon wave functions, $|\varphi_i\rangle$, by superposing Gaussian wave packets, as follows:

$$|\varphi_i\rangle = \sum_{\alpha=1}^{N} \left(\frac{2\nu_\alpha}{\pi}\right)^{3/4} C_\alpha^i \exp\left[-\nu_\alpha \left(\boldsymbol{r} - \frac{\boldsymbol{Z}_\alpha^i}{\sqrt{\nu_\alpha}}\right)^2\right] |\beta_\alpha^i\rangle |\gamma_\alpha^i\rangle, \tag{2·4}$$

$$|\beta_\alpha^i\rangle = \left(\frac{1}{2} + \beta_\alpha^i\right) |\uparrow\rangle + \left(\frac{1}{2} - \beta_\alpha^i\right) |\downarrow\rangle, \tag{2·5}$$

$$|\gamma_\alpha^i\rangle = \left(\frac{1}{2} + \gamma_\alpha^i\right) |p\rangle + \left(\frac{1}{2} - \gamma_\alpha^i\right) |n\rangle, \tag{2·6}$$

where $|\beta_\alpha^i\rangle$ is an intrinsic-spin wave function and $|\gamma_\alpha^i\rangle$ is an isospin wave function. Coefficients C_α^i, β_α^i, γ_α^i and the Gaussian center $\boldsymbol{Z}_\alpha^i$ are complex variational parameters. This single-nucleon wave function, $|\varphi_i\rangle$, is more sophisticated than that in our previous study,[15] where only the spatial part of a single nucleon wave function was expressed by the superposition of Gaussian wave packets, regarding several points. In the present wave function, not only the centers $\{\boldsymbol{Z}_\alpha^i\}$, but also the width parameters $\{\nu_\alpha\}$ of the wave packets are different from each other. Moreover, the variational intrinsic-spin wave function, $|\beta_\alpha^i\rangle$, is independently given for each wave packet. Since the present single-nucleon wave function, $|\varphi_i\rangle$, is possible to describe the strong correlation between the spatial part and the spin part, it can effectively take the contribution from the term $\boldsymbol{\sigma} \cdot \boldsymbol{r}$ in the tensor force, as mentioned in the

previous section. In the isospin part, we also use the variational isospin wave function, $|\gamma_\alpha^i\rangle$, as shown in Eq. (2·6), so that it can contain both the proton and neutron components, though it is fixed to be a proton or neutron state in the usual AMD. Due to the flexibility of the isospin wave function, the present wave function can take effect of the term $\boldsymbol{\tau}_1 \cdot \boldsymbol{\tau}_2$, especially $\tau_{1+}\tau_{2-}$ and $\tau_{1-}\tau_{2+}$, in the tensor force. This corresponds to point ii) mentioned in the previous section.

In our treatment, the total wave function is constructed from an intrinsic wave function, $|\Phi\rangle$, with various projections, where $|\Phi\rangle$ is a Slater determinant of $\{|\varphi_i\rangle\}$: $|\Phi\rangle = \det[|\varphi_i\rangle]$. We performed parity projection ($P_\mathcal{P}$) and angular momentum projection (P_J) in the same way as for the usual AMD calculation for a nuclear structure study. In addition, we need *charge-projection* (P_{T_z}) in the present framework, since $|\Phi\rangle$ is a charge-mixed state, as shown in Eq. (2·6). The charge projection is done by rotating around the z-axis in isospin space,

$$|P_{T_z}\,\Phi\rangle = \int d\alpha \exp\left[i\alpha\left(\hat{T}_z - M\right)\right]\,|\Phi\rangle. \tag{2·7}$$

Thus, the total wave function in the present study is the parity-, angular-momentum- and charge-number-eigen wave function,

$$|P_J P_{T_z} P_\mathcal{P}\,\Phi\rangle. \tag{2·8}$$

Our procedure of energy variation and projections is as follows. We employ $|P_{T_z} P_\mathcal{P}\,\Phi\rangle$ as a trial wave function in the energy variation. The complex variational parameters, $\{X_\alpha^i\} = \{C_\alpha^i,\, \boldsymbol{Z}_\alpha^i,\, \beta_\alpha^i.\gamma_\alpha^i\}$, are determined so as to minimize the energy,

$$\mathcal{H} = \frac{\langle P_{T_z} P_\mathcal{P}\,\Phi|H|P_{T_z} P_\mathcal{P}\,\Phi\rangle}{\langle P_{T_z} P_\mathcal{P}\,\Phi|P_{T_z} P_\mathcal{P}\,\Phi\rangle}, \tag{2·9}$$

by the "frictional cooling method with constraints," which is one of the energy-variation methods. After the energy-variation, $|P_{T_z} P_\mathcal{P}\,\Phi\rangle$ is projected onto the eigenstate of the total angular momentum; $|P_J P_{T_z} P_\mathcal{P}\,\Phi\rangle$. We evaluate various quantities with the wave function $|P_J P_{T_z} P_\mathcal{P}\,\Phi\rangle$.

We here comment on the practical scheme of the frictional cooling method with constraints. As mentioned in Ref. [22], we need a constraint condition to fix the position and momentum of the center of mass ($\langle \mathbf{R}_G\rangle$ and $\langle \mathbf{P}_G\rangle$) to the origin, when a single nucleon wave function is represented by the superposition of several Gaussian wave packets. In the present study, such several constraint conditions are satisfied by adding harmonic-oscillator-type potentials to the energy, $\mathcal{H}$, in the frictional cooling equation:

$$\dot{X}_\alpha^i = (\lambda + i\mu)\frac{\partial \mathcal{H}'}{\partial X_\alpha^{i*}} \quad \text{and C.C.}, \tag{2·10}$$

$$\mathcal{H}' = \mathcal{H} + C_1\left\{\langle \mathbf{R}_G\rangle^2 + \langle \mathbf{P}_G\rangle^2\right\} + \sum_{a=2}^{M} C_a (W_a - W_a^0)^2, \tag{2·11}$$

where W_a and W_a^0 indicate an expectation value of some operator and a constant value, respectively. By adopting adequately large positive constant values of C_1

and C_a in this equation, we can obtain an optimum solution that satisfies several constraint conditions $\{W_a = W_a^0\}$ after frictional cooling. This method works much better than the Lagrange-multiplier method.[15),22)]

§3. Practical results for deuteron and ^{4}He

As explained in §2, we drastically extend the AMD wave function for treating the tensor force. In this section, we show the effect of each extension on the deuteron and ^{4}He.

We consider four extensions: i) a parity-violating mean field and a strong correlation between spin and space, ii) flexibility on the isospin wave function, iii) different width wave packets and iv) charge-, parity- and angular momentum projections. i) and ii) are attributed to the operator form of the tensor force, $(\boldsymbol{\tau}\cdot\boldsymbol{\tau})\ (\boldsymbol{\sigma}_1\cdot\boldsymbol{r})(\boldsymbol{\sigma}_2\cdot\boldsymbol{r})$. Extension i) is effective to the operator $\boldsymbol{\sigma}_i\cdot\boldsymbol{r}$, because this operator changes the parity of a single-particle state and leads to a strong correlation between spin and space. In the AMD method, the former part of i) has already been realized because the parity projection is usually performed. The latter part of i) is taken into account in the present framework by the superposition of Gaussian wave packets that have different spin wave functions. The other operator, $\boldsymbol{\tau}_1\cdot\boldsymbol{\tau}_2$, causes charge-mixing in the single-particle wave function, which is treated by extension ii). We first examine the influence of the tensor force on the properties of the wave function with these extensions. In other words, we look into the perturbative change from the usual model calculations obtained by an effective central-type interaction. Therefore, we use the F-T potential, where the tensor term is added to a central interaction, because such properties as the binding energy and radius of ^{4}He are reproduced with the central term in the F-T potential by simple AMD calculations without any extensions. Next, we adopt the AK(T) potential, which is derived by smoothing out the hard core of the central term in the g-matrix theory based on a realistic nucleon-nucleon potential. In practical calculations with the AK(T) potential, we show that extensions iii) and iv) are important to describe the properties of ^{4}He.

In §§3.1 and §§3.2, we investigate the effects of extensions i) and ii) with the F-T potential, in a simplified model space where the width parameters of all wave packets are set to a common value, namely $\nu_\alpha = \nu$. The effect of extension iii) by using different width parameters is investigated in §§3.3, with the AK(T) potential. In all calculations, the deuteron and ^{4}He are projected onto $J^\pi = 1^+$ and 0^+, respectively.

3.1. *Superposition of Gaussian wave packets with different spins and parity projection*

As mentioned before, in order to treat point i) a parity-violating mean field and strong spin-space correlation in the AMD framework, the parity projection and the superposition of wave packets that have independent spins are needed. We investigated their effects by calculating the deuteron with the F-T potential. Fig. 2(a) shows the binding energy and the expectation value of the tensor force (V_T) for various numbers "N" of wave packets superposed in $|\varphi_i\rangle$. Here, we have fixed each isospin wave function to be a proton or neutron; $|\gamma_\alpha^i\rangle = |p\rangle$ or $|n\rangle$ in Eq. (2·6).

Fig. 2. (a) Binding energy and expectation value of the tensor force (V_T) in the deuteron as a function of the number (N) of wave packets superposed to compose a single nucleon wave function, as described in Eq. (2·4). (b) Expectation value of squared orbital angular momentum in deuteron for various N. The solid (dashed) lines indicate the results with independent (common) intrinsic spins for the wave packets in each single nucleon wave function. Here, the F-T potential is used for both (a) and (b). The details are explained in the text.

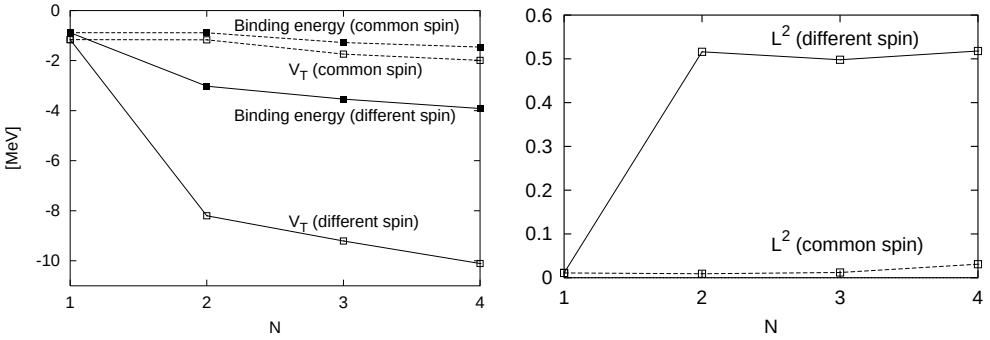

(a) (b)

"common spin" (dashed line) indicates that the common spin wave function is used for all wave packets in each $|\varphi_i\rangle$, namely $|\beta_\alpha^i\rangle = |\beta^i\rangle$ in Eq. (2·4), whereas "different spin" (solid line) indicates that each wave packet independently has a different spin wave function, as shown in Eq. (2·4).

As shown in the figure, the expectation value of the tensor force, which we denote as $|V_T|$, is nearly equal to zero when the superposition of wave packets is not performed ($N = 1$). In the case that different spin wave functions are used for each wave packet, $|V_T|$ is increased and the binding energy is gained by the superposition (see the $N \geq 2$ region of "different spin" in Fig. 2(a)). A drastic energy gain of the V_T term is seen when the number of wave packets (N) is changed from 1 to 2. On the other hand, when we use a common spin wave function for each wave packet, $|V_T|$ remains to be nearly zero, even if more than two wave packets are used ($N \geq 2$ and "common spin"). In order to see the mixing ratio of high-angular-momentum components, we show the expectation value of the squared orbital angular momentum, $\boldsymbol{L}^2 \equiv \langle \hat{\boldsymbol{L}}^2 \rangle$, of the total system in Fig. 2(b). Corresponding to the behavior of V_T, $\boldsymbol{L}^2$ is also drastically deviated from zero in the case that a different spin wave function is used (solid line). This deviation of $\boldsymbol{L}^2$ from zero indicates a mixing of the D-state, which is consistent with the usual understanding of the deuteron, that the tensor force is gained by ${}^3S_1$-${}^3D_1$ coupling. Thus, we found that, in the description of a single nucleon wave function, $|\varphi_i\rangle$, the superposition of more than two Gaussian wave packets with independent spin wave functions is effective to gain the tensor force in the AMD framework.

Since the operator $\boldsymbol{\sigma}_i \cdot \boldsymbol{r}$ changes the parity of a single-particle state, a parity-violated single-particle state is necessary to incorporate the effect of this operator. In order to properly take into account the parity violation of single-particle wave functions, the parity projection before the variation of the total system is important. We show the effect of the parity projection in the deuteron in Table I. In the upper

row ("w"), we show the result with the parity projection, which corresponds to $N = 4$ wave packets with different spins in Fig. 2(a). The lower row ("w/o") shows the expectation values for the wave function obtained by switching off the parity projection. The contribution of the tensor force without the parity projection (-1.5 MeV) is much smaller than that of the result with the parity projection (-10.1 MeV). $\boldsymbol{L}^2$ is also reduced from 0.52 to 0.05, which means a decrease of the D-state mixing by switching off the projection. Thus, we confirm the importance of the parity projection. For the deuteron calculated with parity projection, its single nucleon wave function is actually a parity-violated state with the mixing of s- and p-orbits, as shown in §4.

3.2. *Flexibility on the isospin wave function and charge projection*

We calculate the ^{4}He by using F-T potential, and investigate the effect of the point ii) flexibility of the isospin wave function. The results are summarized in Table II. In calculations except for "Usual AMD", each single nucleon wave function is described by four wave packets ($N = 4$) with independent intrinsic spin functions (different spins). The top row ("Usual AMD") is obtained by the ordinary version of AMD, in which each nucleon is described with a single wave packet, and parity and angular-momentum projections are performed. The middle row ("Isospin fixed") is obtained by a calculation in which each isospin wave function, $|\gamma_\alpha^i\rangle$, is fixed to be a proton or neutron, $|\gamma_\alpha^i\rangle = |p\rangle$ or $|n\rangle$, in the same way as the calculation of the deuteron. The bottom row ("Isospin free") is obtained by a calculation in which $|\gamma_\alpha^i\rangle$ can describe a proton-neutron mixed state, $|\gamma_\alpha^i\rangle = \left(\frac{1}{2} + \gamma_\alpha^i\right)|p\rangle + \left(\frac{1}{2} - \gamma_\alpha^i\right)|n\rangle$, with the variational parameter γ_α^i, as shown in Eq. (2·6). By comparing these results, $|V_T|$ and $\boldsymbol{L}^2$ are larger in the case of "Isospin free" than in the case of "Isospin fixed". Therefore, it is found that the use of the isospin-mixed single nucleon wave function is important to gain the tensor force in ^{4}He.

In the previous and present subsections, we qualitatively show that two extensions of the AMD framework, i) a parity-violating mean field and a strong correlation between spin and space and ii) flexibility of the isospin wave function, are necessary to treat the tensor force. However, the results obtained by the F-T potential still fail to quantitatively reproduce the experimental values of such properties as the binding energies and the root-mean-square radii of these nuclei. Both of the deuteron and ^{4}He are overbound and overshrunk, as can be seen in Table I and II.

We consider that these failures are caused by the too-large contribution of the central term of the F-T potential. Due to the extension of the AMD framework, the

Table I. Effect of parity projection in the deuteron, which is calculated with the F-T potential. The upper (lower) row shows the result obtained with (without) parity projection. T, V_C, V_T and B.E. are the kinetic energy, central force, tensor force and total binding energy, respectively. They are in units of MeV. $\boldsymbol{L}^2$ is the expectation value of the squared orbital angular momentum.

Parity projection	T	V_C	V_T	B.E.	$\boldsymbol{L}^2$
w	24.3	-18.1	-10.1	3.9	0.52
w/o	16.0	-15.7	-1.5	1.2	0.05

contribution of the tensor force becomes large, as we expected. However, as shown in "Usual AMD" in Table II, the central force in the F-T potential is so strong that ^{4}He is already sufficiently bound without any attraction by the tensor force. As a result of the large contribution of the tensor force gained by the extended framework in addition to such large contribution of the central force, overbinding and shrinkage occur. We can explain these failures as being attributed to a mismatching between the extended model space of the present framework and the F-T potential. The F-T potential should be used in a simple model space, as written in the original paper.[19] In a simple model space, an explicit tensor term has only a minor effect, while the dominant contribution of the original tensor force is renormalized into the large attraction of the central term in the F-T potential. It can well reproduce the total binding energy of ^{4}He when it is used in a small model space. In the case of the present calculation, due to the relatively large model space of the extended AMD, the contribution of the tensor force becomes large. Consequently, since the tensor force is already renormalized into the central force, it is doubly counted in the central term and in the direct tensor term, causing such overbinding.

3.3. *Different width wave packets and angular-momentum projection*

As explained in the former subsection, we can not quantitatively reproduce the properties of the deuteron and ^{4}He with the F-T potential, which has a strong ^3E central force. Since this potential is not suitable for our research strategy, where we treat the tensor force directly without renormalizing into the central force, we employ another type of potential based on the AK(T) potential, in which the magnitude of the ^3E central force is nearly equal to that of the tensor force. We think that the AK(T) potential is more suitable to the extended AMD framework than the F-T potential, because the tensor force is not renormalized into the central force. As discussed in Ref. [5], the matrix element of the tensor force is reduced approximately by a factor of $\sqrt{\frac{1}{2}}$ in simple mean-field approaches. Therefore, we enhance the strength of the tensor force by some factor also in the case of AMD in order to properly evaluate the matrix element of the tensor force. In the present calculation, we phenomenologically make the strength of the tensor force in the original AK(T) potential twice enhanced, so as to reproduce the binding energy and radius of ^{4}He.

We calculated ^{4}He with the AK(T) potential under various conditions of the model space and the variation, and investigated the effect of different width wave

Table II. Results of ^{4}He with the F-T potential. T, V_C, V_{LS}, V_T, V_e and B.E. are the kinetic energy, central force, LS force, tensor force, Coulomb force and total binding energy, respectively. They are in units of MeV. $\boldsymbol{L}^2$ is the expectation value of the orbital angular momentum. R_{rms} is the root-mean-square radius of the system in units of fm. The experimental values of the binding energy and R_{rms} of ^{4}He are B.E. = 28.3 MeV and R_{rms} = 1.47 fm.[23]

	T	V_C	V_{LS}	V_T	V_e	B.E.	$\boldsymbol{L}^2$	R_{rms}
Usual AMD	56.0	−85.3	0.0	−1.7	0.9	30.1	0.01	1.37
Isospin fixed	57.4	−85.7	0.2	−4.2	0.9	31.4	0.06	1.36
Isospin free	77.6	−96.2	2.1	−22.4	1.0	37.9	0.41	1.22

packets (point iii)) and that of the angular momentum projection (an ingredient of the point iv)). We list the conditions I $\sim$ V' in Table III. Except for case V', the single-nucleon wave functions are represented with four wave packets, which corresponds to the case $N = 4$ in Eq. (2·4). We perform the calculation of ^{4}He with a common width parameter for all packets (I, II: ν's="com.") and with different width parameters of wave packets (III, IV: ν's="diff."). In the former case "com.", a common width parameter $\nu_\alpha = \nu$ is used, and is chosen to be $\nu = 0.6$ so as to minimize the energy of ^{4}He. In the latter case of different widths ("diff."), ν_α is given as

$$\nu_\alpha = \nu_1 \times (\nu_N/\nu_1)^{\frac{\alpha-1}{N-1}} . \tag{3·1}$$

After some trials of various sets $\{\nu_1, \nu_4\}$, we found the optimum set, $\nu_1 = 0.3$ and $\nu_4 = 1.5$, which gives the energy minimum. The adopted width parameters $\{\nu_\alpha\}$ are listed in Table III. In each case of a common width (I, II) and different widths (III, IV), we first performed the energy variation without the angular-momentum (J) projection (I, III), and projected the obtained wave functions onto the J-eigen states (II, IV).

The results of ^{4}He calculated under each condition are given in Table IV. By comparing II (a common width) and IV (different widths), it is found that the reproduction of both the binding energy and the radius is improved in result IV.

Table III. Summary of conditions in calculating ^{4}He with the AK(T) potential. "N" means the number of wave packets for a single nucleon wave function. "ν's" indicates that the width parameters of the wave packets are equal to ("com.") or different from each other ("diff."). "$\nu_1 \sim \nu_5$" show values of the adopted width parameters in units of fm^{-2}. "J pro." indicates that the angular momentum projection has been done ("w") or not ("w/o"). "w/o" in "J const." means that a solution is obtained by the usual frictional cooling method without a J constraint. We constructed a better solution by the frictional cooling method with the J constraint ("w" in "J const."). A detailed explanation is given in the text.

	N	ν's	ν_1	ν_2	ν_3	ν_4	ν_5	J pro.	J const.
I	4	com.	0.60	0.60	0.60	0.60	—	w/o	w/o
II	4	com.	0.60	0.60	0.60	0.60	—	w	w/o
III	4	diff.	0.30	0.51	0.88	1.50	—	w/o	w/o
IV	4	diff.	0.30	0.51	0.88	1.50	—	w	w/o
V	4	diff.	0.30	0.51	0.88	1.50	—	w	w
V'	5	diff.	0.30	0.45	0.67	1.00	1.50	w	w

Table IV. Results of ^{4}He with the AK(T) potential calculated under various conditions. The conditions "I $\sim$ V' " correspond to TABLE III. $\boldsymbol{J}^2$, $\boldsymbol{L}^2$ and $\boldsymbol{S}^2$ are the expectation values of the total angular momentum, the orbital angular momentum and the spin, respectively.

	T	V_C	V_T	V_e	B.E.	R_{rms}	$\boldsymbol{J}^2$	$\boldsymbol{L}^2$	$\boldsymbol{S}^2$
I	94.1	−39.4	−66.4	0.9	10.8	1.23	0.32	1.50	1.31
II	91.7	−40.3	−68.0	0.9	15.7	1.23	0.00	1.27	1.27
III	79.0	−41.9	−55.4	0.9	17.4	1.32	0.23	0.80	0.68
IV	73.4	−43.5	−56.2	0.9	25.3	1.32	0.00	0.57	0.57
V	70.4	−43.5	−56.3	0.9	28.6	1.35	0.00	0.50	0.51
V'	69.0	−43.0	−55.5	0.9	28.7	1.35	0.00	0.54	0.54

This shows the importance of using wave packets with different widths.

The comparison of III (without J projection) and IV (with J projection) indicates the importance of the angular-momentum projection. As can be seen in Table IV, the binding energy gains 8 MeV in result IV by the J projection. Before the J projection, the $\boldsymbol{J}^2$ value is small, as can be seen in result III, which indicates that the $J \neq 0$ components are very small. Considering that the state is almost the $J = 0$ eigen state already before the J projection, the energy gain by the projection seems to be unexpectedly large. This gain is dominantly attributed to a decrease of the kinetic energy term. Dissolving the III state ($|\Phi_{\rm III}\rangle$) into various (J, J_z) components ($|J\,J_z\rangle$), we analyzed the contributions of each (J, J_z) component to the kinetic energy (Table V). Detailed expressions of $|\Phi_{\rm III}\rangle$ and $|J\,J_z\rangle$ are

$$|\Phi_{\rm III}\rangle \equiv P_{Tz=0}\,P_{P=+}\,|\Phi\rangle, \tag{3·2}$$

$$|J\,J_z\rangle \equiv P_{J,Jz}\,|\Phi_{\rm III}\rangle, \tag{3·3}$$

where $|\Phi\rangle$ is the intrinsic state of the III state. As shown in Table V, the $J = 0$ component is dominant as 96%, while the $J = 1$ and $J = 2$ components are mixed into the III state at the rate of a few percent. Although the $J = 1$ and 2 components are very small, they have huge kinetic energy ($\simeq 200$ MeV), and hence the significant gain of the kinetic energy is caused by excluding the $J \neq 0$ components after the J projection. Such a huge kinetic energy of the $J \neq 0$ components arise from very narrow wave packets, such as $\nu_4 = 1.5$ used in calculating III and IV. It is considered that high-momentum components are contained in the $J \neq 0$ components of the III state, due to such narrow wave packets.

Since our calculation procedure is "Variation Before Projection" with respect to the J projection, we can expect to find a better solution of the $J = 0$ state than IV. For this aim, we apply a constraint condition method in the present framework. We put a constraint on the squared total angular momentum by setting $W_2 = \langle \hat{\boldsymbol{J}}^2 \rangle$ in the Eq. (2·11) for the energy variation, and constructed the states with various values of $\langle \hat{\boldsymbol{J}}^2 \rangle$ ($\hat{\boldsymbol{J}}$ is the total angular momentum operator). After the energy variation, we

Table V. Contributions from various J components to the kinetic energy. "Before J projection" corresponds to the III state in Table IV. "overlap" indicates the ratio of each (J, J_z) component ($|J\,J_z\rangle$) included in the III state ($|\Phi_{\rm III}\rangle$); $|\langle J\,J_z|\Phi_{\rm III}\rangle|^2/\sqrt{\langle J\,J_z|J\,J_z\rangle\langle\Phi_{\rm III}|\Phi_{\rm III}\rangle}$. The definitions of $|\Phi_{\rm III}\rangle$ and $|J\,J_z\rangle$ are explained in the text.

J	J_z	T	overlap	$T \times$ overlap
Before J projection		79.04	—	—
0	0	73.43	0.955	70.09
1	1	199.75	0.007	1.38
1	0	—	0.000	0.00
1	−1	201.24	0.007	1.35
2	2	238.19	0.005	1.23
2	1	172.96	0.002	0.31
2	0	—	0.000	0.00
2	−1	177.75	0.002	0.30
2	−2	238.38	0.005	1.24

projected them onto the $J = 0$ state and obtained an energy surface as a function of the value of the constraint $\langle \hat{\boldsymbol{J}}^2 \rangle$. We then chose the energetically best solution, which is state "V" shown in Table IV. In this solution, the binding energy and the radius are more improved than IV. In this final result, V, the binding energy and the radius are -28.6 MeV and 1.35 fm, respectively. We checked the convergence of the solution with an increase of the number of wave packets, N. V' is the result obtained by using five wave packets for each nucleon wave function, namely $N = 5$ in Eq. (2·4), in the same way as the case of V for $N = 4$. Since the changes of various properties from the V state to the V' state are very small, we consider that the convergence of the solution is sufficient at $N = 4$.

Thus, we confirmed that extension iii) *different width wave packets* and especially the *angular-momentum projection* in iv) are effective as well as extensions i) and ii).

3.4. *Systematics of deuteron, triton and alpha with AK(T) potential*

Within the extended AMD framework we could rather quantitatively reproduce the properties of ^{4}He by using the AK(T) potential with a twice-enhanced strength of the tensor term. We now consider our calculation of the deuteron and triton in the same way as in case V for ^{4}He. The results are given in Table VI. Comparing the theoretical values of binding energies and radii with the experimental data, we can tolerate the result of the triton, though it is somewhat overbound, whereas the deuteron is terribly overbound and overshrunk.

One of the reasons for this failure in systematic reproduction is conjectured to be as follows: The deuteron is a special system, because it is composed of only two nucleons. It has just one degree of freedom in the spatial coordinate, namely, the relative motion between them. Since its relative motion may be described sufficiently well by the superposition of Gaussian wave packets in the extended AMD, the two-body correlation in the deuteron is incorporated much better than that in ^{4}He. As mentioned in the previous section, Ref. [5] pointed out that the matrix element of the tensor force is reduced approximately by a factor of $\sqrt{\frac{1}{2}}$ in the simple mean-field type treatment of ^{4}He due to the limitation of the model space, which is insufficient to incorporate a two-body correlation. In order to regain this reduction, we need a

Table VI. Results of the deuteron, triton and ^{4}He calculated with AK(T) potential. "N" means the number of wave packets for a single nucleon wave function. "x_T" indicates the enhancement factor of the strength of the tensor force. "a_1", "b" and "c" show the results of the deuteron, triton and ^{4}He calculated with the twice-enhanced tensor force. "a_2" is the deuteron calculated with a 1.5-times enhanced tensor force. The experimental values of the binding energy and radius: B.E. = 2.2 MeV and $R_{rms} = 1.94$ fm for deuteron, and 8.5 MeV and $R_{rms} = 1.55$ fm for triton.[23)]

		N	x_T	T	V_C	V_T	V_e	B.E.	R_{rms}	$\boldsymbol{J}^2$	$\boldsymbol{L}^2$	$\boldsymbol{S}^2$
a_1	^{2}H	5	2.0	34.9	-4.1	-44.1	0.0	13.4	1.00	2.00	0.72	1.98
a_2	^{2}H	5	1.5	23.2	-4.2	-20.7	0.0	1.7	1.19	2.00	0.49	1.99
b	^{3}H	5	2.0	48.0	-20.5	-38.0	0.0	10.5	1.27	0.75	0.54	1.01
c	^{4}He	4	2.0	70.4	-43.5	-56.3	0.9	28.6	1.35	0.00	0.50	0.51

twice-stronger tensor force for the calculation of ^{4}He. However, because of the better description of the two-body correlation in the deuteron wave function than in ^{4}He, the reduction factor of the matrix element must be smaller and the enhancement factor of the strength should be smaller in the deuteron than in ^{4}He. This means that the twice-enhanced tensor force is too strong for the deuteron. Actually, from the value $\boldsymbol{L}^2 = 0.72$ shown in row "a_1", we can find that the D-state probability of the deuteron is too large (about 12%), compared with the well-known value of several %. We then calculated the deuteron with a smaller enhancement factor, $x_T = 1.5$, of the strength of the tensor force. The result is shown in row "a_2" of Table VI. In this case, $\boldsymbol{L}^2 = 0.49$, which indicates that the D-state probability is estimated to be a reasonable value as 8%. The binding energy also decreases to be 1.7 MeV, which well agrees with the experimental data. These results support that an about 1.5 time enhancement of the tensor force is suitable to reproduce structure properties in the case of the deuteron system.

§4. Analysis of and discussion on single particle levels

The ^{4}He obtained by the extended version of AMD with the AK(T) potential has a significant contribution of the tensor force to the potential energy. Due to the tensor force, the obtained wave function is expected to be more complicated than the ordinary $(0s)^4$-like wave function obtained with the usual effective forces with no tensor term. In this section, we clarify its internal structure.

In the procedure of the present calculation to obtain a total wave function, we operate parity-, charge- and angular-momentum-projections to an intrinsic wave function. The wave function of ^{4}He is written as

$$|^4\mathrm{He}\rangle \;=\; P_{J=0}\, P_{T_z=0}\, P_{\mathcal{P}=+}\, |\Phi\rangle, \tag{4·1}$$

where the intrinsic state, $|\Phi\rangle$, is expressed by a single Slater determinant. We can analyze the Hartree-Fock-like single-particle orbits, $|\alpha_i\rangle$ $(i = 1 \sim 4)$, (AMD-HF orbits) extracted from the AMD wave function, $|\Phi\rangle$, by the method given in Ref. [22].

Table VII shows the properties of the AMD-HF levels extracted from the intrinsic wave function of result V in Table IV. Apparently, the intrinsic state $|\Phi\rangle$ is not the simple $(0s)^4$ state. If $|\Phi\rangle$ were the $(0s)^4$ state, $\boldsymbol{j}^2$, $\boldsymbol{l}^2$ and $P(+)$ should be equal

Table VII. Single particle levels of ^{4}He in the state V. "S.P.E." is the single particle energy of each level in unit of MeV. "$\boldsymbol{j}^2$" and "$\boldsymbol{l}^2$" are the expectation value of total angular momentum and orbital angular momentum, respectively. "P(+) (P(−))" and "P(proton) (P(neutron))" are the ratio of the positive(negative) parity component and the proton(neutron) component included in each level, respectively. They are in unit of %.

Level	S.P.E.	$\boldsymbol{j}^2$	$\boldsymbol{l}^2$	P(+)	P(−)	P(proton)	P(neutron)
1	−4.04	1.16	0.83	81	19	61	39
2	−4.52	1.17	0.85	81	19	59	41
3	−8.28	1.09	0.68	85	15	30	70
4	−8.78	1.06	0.65	86	14	45	55

to 0.25, 0.00 and 100% at each level, respectively. The obtained values, however, deviate from these values. The obtained levels contain a negative-parity component with $15 \sim 20\%$, and $\boldsymbol{l}^2$ is non-zero. These results indicate a mixture of the p state in all single-particle orbits. It is interesting that they are also proton-neutron-mixed states, as shown in Table VII.

To investigate in more detail, we have decomposed the AMD-HF level into the eigen-state of parity and charge. The composition of each level is shown in Table VIII. $\boldsymbol{l}^2$ and the root-mean-square radius of each component are given in Table IX and X, respectively. The negative-parity components included in all AMD-HF levels are found to be dominated by p orbits, because $\boldsymbol{l}^2$ for the negative-parity component for both of proton and neutron is nearly equal to 2, as shown in Table IX. In the positive-parity components, non-zero $\boldsymbol{l}^2$ values imply the mixing of d orbits with the dominant s orbit. As shown in Table X, the radius of the negative-parity components is about 1.28 fm. If we assume a harmonic-oscillator wave function, this radius, 1.28 fm, of the p-orbits suggests an unusually small oscillator size. On the other hand, the radius of the positive-parity components is about 1.6 fm, which suggests a normal size for the s obit in ^{4}He. Thus, it is considered that the *narrow p state* (negative-parity component) is mixed with the normal-size s state (positive-parity component) in each level.

In order to confirm the above picture, we analyze the AMD-HF orbits with

Table VIII. Composition of the single-particle levels. proton (neutron) + (−) means the component of the proton (neutron) with the positive (negative) parity. The values are in unit of %.

Level	proton +	neutron +	proton −	neutron −
1	55	26	6	13
2	50	30	9	10
3	21	64	9	6
4	37	49	8	6

Table IX. Expectation value of $\boldsymbol{l}^2$ of each component.

Level	proton +	neutron +	proton −	neutron −
1	0.16	0.99	2.58	2.56
2	0.29	0.64	2.61	2.61
3	1.09	0.10	2.68	2.63
4	0.41	0.26	2.67	2.48

Table X. Root-mean-square radius of each component. The units are fm.

Level	proton +	neutron +	proton −	neutron −
1	1.59	1.70	1.30	1.27
2	1.58	1.60	1.27	1.31
3	1.55	1.54	1.26	1.28
4	1.52	1.51	1.28	1.25

Fig. 3. Overlaps between the AMD-HF states extracted from state V in Table IV and the s and p states in the harmonic-oscillator potential with various width parameters (ν_s and ν_p fm^{-2}). (a) Overlap between the positive parity component of each AMD-HF state and the s state; $|\langle s_{\rm H.O.}|\alpha_i^+\rangle|^2$. (b) Overlap between the negative parity component of each AMD-HF state and the p state; $|\langle p_{\rm H.O.}|\alpha_i^-\rangle|^2$. The four lines in each figure correspond to four single-particle levels, respectively.

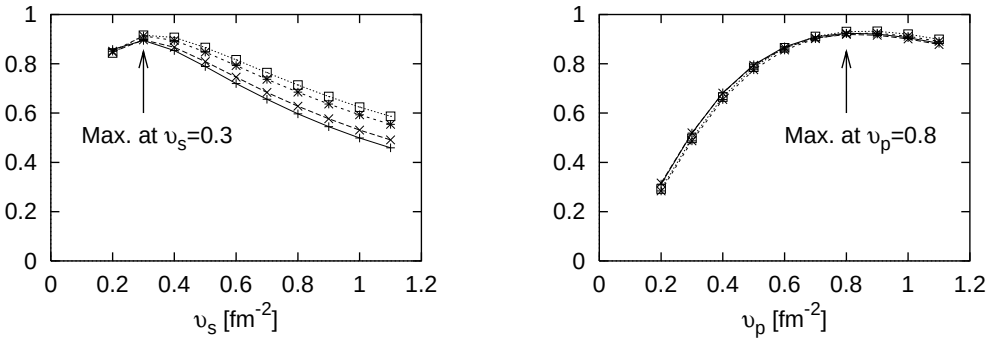

(a) positive parity (b) negative parity

simple s- and p-orbits written in terms of harmonic-oscillator (H.O.) wave functions:

$$|s_{\rm H.O.}\rangle: \quad \langle \boldsymbol{r}|0s_{\frac{1}{2}},m,\tau_z\rangle = R_s(r)\left|\frac{1}{2},m\right\rangle\cdot\left|\frac{1}{2},\tau_z\right\rangle, \tag{4·2}$$

$$R_s(r) = N_s^{-\frac{1}{2}}\exp\left[-\nu_s r^2\right], \tag{4·3}$$

$$|p_{\rm H.O.}\rangle: \quad \langle \boldsymbol{r}|0p_j,m,\tau_z\rangle = R_p(r)\left[\sum_{m_l,m_s}\left(1m_l,\frac{1}{2}m_s|jm\right)Y_{1m_l}(\Omega)\left|\frac{1}{2},m_s\right\rangle\right]\cdot\left|\frac{1}{2},\tau_z\right\rangle, \tag{4·4}$$

$$R_p(r) = N_p^{-\frac{1}{2}}\,r\,\exp\left[-\nu_p r^2\right]. \tag{4·5}$$

Here, ν_s and ν_p indicate the width parameters of the s and p orbits, respectively. Fig. 3(a) (3(b)) shows the overlap between the positive (negative)-parity component of the AMD-HF states, $|\alpha_i^{\pm}\rangle$, and the $s_{\rm H.O.}$ ($p_{\rm H.O.}$) state as a function of the H.O. width parameter, ν_s (ν_p). Here, $|\alpha_i^{\pm}\rangle$ is the parity-eigen state projected from $|\alpha_i\rangle$,

Table XI. Composition of the p state at $\nu_p = 0.8$ fm^{-2}. The units are %. "p" and "n" in the column "p or n" mean the proton and neutron component, respectively. "p+n" means the sum of proton and neutron components.

	p or n	level 1	level 2	level 3	level 4
$0p_{\frac{1}{2}}$	p	27.2	41.3	54.8	48.0
$0p_{\frac{1}{2}}$	n	59.8	43.6	32.4	39.2
$0p_{\frac{1}{2}}$	p+n	87.0	84.9	87.2	87.3
$0p_{\frac{3}{2}}$	p	2.0	2.9	3.3	3.6
$0p_{\frac{3}{2}}$	n	3.4	4.0	1.8	2.2
$0p_{\frac{3}{2}}$	p+n	5.4	6.9	5.1	5.8
$0p$	p+n	92.4	91.8	92.3	93.1

Fig. 4. Comparison of the radial dependence of the single-particle wave functions and the tensor force. "$R_s * R_p$" (dashed line) is the product of the radial wave function of the s state (Eq. 4·3) and that of the p state (Eq. 4·5). "V_T" (solid line) is the radial part of the tensor force of the AK(T) potential. Both are depicted after being multiplied by r^2.

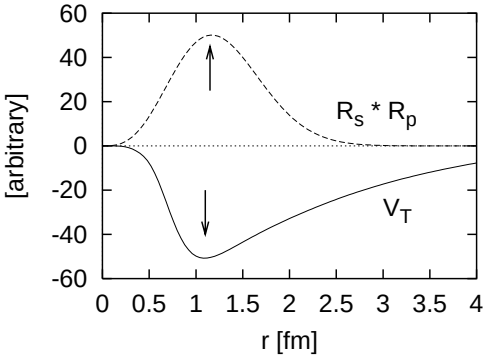

where $\langle \alpha_i^{\pm} | \alpha_i^{\pm} \rangle = 1$. $|s_{\text{H.O.}}\rangle$ and $|p_{\text{H.O.}}\rangle$ have maximum overlap (92%) with $|\alpha_i^+\rangle$ and $|\alpha_i^-\rangle$ at $\nu_s = 0.3$ fm^{-2} and $\nu_p = 0.8$ fm^{-2}, respectively. On the other hand, the typical width parameter, $\nu = 0.26$ fm^{-2}, is known to reproduce the size of ^{4}He by the H.O. $(0s)^4$ wave function. Thus, it is explicitly confirmed that the narrow p state is mixed with the normal-size s state. It is worth showing that the 92% $0p$ state consists of 86% $0p_{\frac{1}{2}}$ and 6% $0p_{\frac{3}{2}}$ (Table XI).

The reason for the mixture of such a shrunk p orbit can be understood as follows. In the single-particle picture, the matrix element of the tensor force is gained by the coupling of the s state and the p state, such as $\langle\, [pp]d \,|v_{12}^T|\, [ss]s \,\rangle$ in which two nucleons in the p orbit and those in the s orbit are coupled to the d orbit and the s orbit, respectively. Fig. 4 shows the product of the radial wave functions of the $s_{\text{H.O.}}$ orbit ($\nu_s = 0.3$) and the narrow $p_{\text{H.O.}}$ orbit ($\nu_p = 0.8$), and also the radial part of the tensor force in the AK(T) potential. The peak position of the product of these two orbits is consistent with the potential range of the tensor force. Such a combination as $s_{\text{H.O.}}(\nu_s = 0.3)$ and $p_{\text{H.O.}}(\nu_p = 0.8)$ is suitable to incorporate the tensor effect into the binding energy. As a result of the analysis of the single particle levels, we are convinced of the role of extension iii). In other words, we should use wave packets with different width parameters in order to describe the shrunk p orbit simultaneously with the normal-size s orbit.

§5. Summary

In the present paper, we tried to construct a new model that can treat the tensor force directly, based on the antisymmetrized molecular dynamics method (AMD). We employed the Furutani-Tamagaki potential (F-T potential) and the Akaishi(T) potential (AK(T) potential). As a result of practical calculations, we confirmed that four extensions in the AMD framework are effective for a direct treatment of the tensor force: i) a parity-violating mean field and a strong correlation between spin and space, ii) flexibility on the isospin wave function, iii) different width wave

packets and iv) charge-, parity- and angular-momentum-projections. Due to all of the above extensions, we obtained a satisfactory solution of ^{4}He. We can reproduce the binding energy for ^{4}He with the AK(T) potential with a twice-enhanced tensor strength; also, the radius of the calculated ^{4}He well agrees with the experimental value; The binding energy and root-mean-square radius were calculated to be 28.6 MeV and 1.35 fm, respectively. The energy composition is as follows: $T = 70.4$ MeV, $V_C = -43.5$ MeV, $V_T = -56.3$ MeV and $V_{Coulomb} = 0.9$ MeV. Thus, this solution has a large contribution of the tensor force, as we expected. We found that the influence of the large contribution of the tensor force appeared in single-particle wave functions of this ^{4}He solution. The shrunk p orbit was mixed to the usual $0s$ orbit to gain the tensor force.

We could gain a large contribution of tensor force in the deuteron, triton and ^{4}He with the extended version of AMD. However, we are not satisfied with the results because we need a two-fold enhancement of the tensor force in the AK(T) potential to quantitatively describe the properties of ^{4}He, and have not yet succeeded to reproduce the systematics of the binding energies of the deuteron, triton, and ^{4}He. These fact may mean that the extension of the framework is still insufficient. Referring to the deuteron system, we here comment on possible residual correlations. Since the deuteron has only one degree of freedom, i.e. the relative motion, the description of the two-body correlation is considered to be directly improved by increasing the number of wave-packets. In fact, we have found that the tensor contribution in the deuteron changes drastically with an increase of the number of wave packets from $N = 5$ to 10, with its binding energy changing from 13.4 MeV to 18.2 MeV. It is different from the case of ^{4}He, where the results almost converge at $N = 4$. In the case of $N = 10$ for the deuteron, only a 1.4-times enhancement of the tensor force is sufficient to get the satisfactory result of 1.6 MeV for the deuteron binding energy, which agrees with the experimental data (2.2 MeV). This result implies that there is some scope to improve the description of the two-body correlation in our framework. In a mean-field-type model, such as the AMD method, it is difficult to treat the short-range part of the tensor force. This difficulty is expected to be overcome by introducing the so-called T-type base,[24] or renormalizing such a part of the tensor force into the central force. In order to perform further studies based on AMD, the latter way is suitable for our method. Due to renormalization of the short-range tensor force, the central force is expected to become more attractive than the present one. From the result obtained with the F-T potential, which has a strong central force, we can conjecture that the binding energy is easily reproduced by the renormalized force without the enhancement factor of the tensor force. In a study with a mean-field approach by Sugimoto *et al.*,[12] they use the enhancement factor 1.5 for the same tensor force as in the present study. By adjusting the strength of the central force, the binding energy of ^{4}He is well described in their study. Although the central force is phenomenologically fitted, their approach is interpreted to simulate the above-mentioned renormalization of the short-range tensor force in the central force. Needless to say, it is important to derive effective nuclear interactions with a direct long-range part and a renormalized short-range part of the tensor force based on realistic forces, as much as possible.

Such a renormalization framework may work effectively to investigate the influence of the tensor force on the nuclear structure, because the short-range part of tensor force is expected to affect mainly the bulk properties of nuclei, while its long-range part should be sensitive to the details of the nuclear structure.

Acknowledgements

One of the authors (A. D.) thanks Dr. S. Sugimoto for fruitful discussions and his encouragement. He is very thankful to Prof. A. Tohsaki and Dr. M. Kimura for their advice on a mathematical technique. This work is supported by JSPS Research Fellowships for Young Scientists, and was performed under the Research Project for Study of Unstable Nuclei from Nuclear Cluster Aspect, sponsored by the Institute of Physical and Chemical Research (RIKEN).

Appendix

Parameters in the Akaishi(T) potential are given in Table XII. C_n^{1E}, C_n^{3E}, C_n^{1O} and C_n^{3O} are parameters of the central force in Eq. (2·2) and T_n^{3E} is that of the tensor force in Eq. (2·3). Each range parameter, b_n, is generated from b_1 and b_{10} by $b_n = b_1 \times (b_{10}/b_1)^{(n-1)/9}$.

Table XII. Range parameters $\{b_n\}$ and coefficients $\{C_n^X\}$ in v_{ij}^C and $\{T_n^X\}$ in v_{ij}^T of AK(T) potential. The units of $\{b_n\}$, $\{C_n^X\}$ and $\{T_n^X\}$ are fm, MeV and MeV/fm^2, respectively. The definitions are given in Eqs. (2·2) and (2·3).

n	b_n	C_n^{1E}	C_n^{3E}	C_n^{1O}	C_n^{3O}	T_n^{3E}
1	0.1600	-3.4970×10^2	-3.2879×10^2	2.7042×10^1	1.5355×10^2	-2.2053×10^2
2	0.2141	1.4440×10^3	1.2518×10^3	-2.0400×10^2	-1.2405×10^2	1.1121×10^3
3	0.2865	-2.9647×10^3	-2.5066×10^3	9.0073×10^2	-5.1523×10^2	-1.6079×10^3
4	0.3833	1.4499×10^3	1.3850×10^3	-1.8442×10^3	4.7590×10^2	1.3446×10^2
5	0.5129	1.6601×10^3	1.2147×10^3	1.3668×10^3	4.3360×10^2	-3.8447×10^2
6	0.6863	-7.7942×10^2	-6.5449×10^2	1.8709×10^1	2.5416×10^1	-1.8164×10^2
7	0.9183	-1.4783×10^1	7.6192×10^1	8.5685×10^1	-4.6085×10^1	-4.1188×10^1
8	1.229	-6.1748×10^1	-6.5063×10^1	-3.5048×10^{-1}	4.3151	-1.2277×10^1
9	1.644	6.5369	1.1420×10^1	-6.3206	-6.8892	-2.2104
10	2.200	-6.4642	-6.6031	1.3007×10^1	1.6804	-6.5291×10^{-1}

References

1) R. B. Wiringa, S. C. Pieper, J. Carlson and V. R. Pandharipande, Phys. Rev. C **62** (2000), 014001.
2) H. Kamada *et al.*, Phys. Rev. C **64** (2001), 044001.
3) T. Terasawa, Prog. Theor. Phys. **23** (1960), 87; A. Arima and T. Terasawa, Prog. Theor. Phys. **23** (1960), 115; S. Nagata, T. Sasakawa, T. Sawada, and R. Tamagaki, Prog. Theor. Phys. **22** (1959), 274.
4) Y. Akaishi and S. Nagata, Prog. Theor. Phys. **48** (1972), 133; Y. Akaishi, H. Bando and S. Nagata, Prog. Theor. Phys. Suppl. No. 52 (1972), 339.
5) T. Myo, K. Kato and K. Ikeda, Prog. Theor. Phys. **113** (2005), 763.

6) H. Toki, S. Sugimoto and K. Ikeda, Prog. Theor. Phys. **108** (2002), 903. H. Toki, Y. Ogawa, S. Tamenaga, S. Sugimoto and K. Ikeda, Nucl. Phys. **A738** (2004), 87.
7) H. A. Bethe, Annu. Rev. Nucl. Sci. **21** (1971), 93.
8) T. Myo, K. Kato, H. Toki, and K. Ikeda, private communication.
9) T. Neff and H. Feldmeier, Nucl. Phys. A **713** (2003), 311.
10) Y. Akaishi, Nucl. Phys. **A738** (2004), 80.
11) S. K. Bogner, T. T. S. Kuo and A. Schwenk, Phys. Rep. **386** (2003), 1.
12) S. Sugimoto, H. Toki and K. Ikeda, Nucl. Phys. **A738** (2004), 240; Nucl. Phys. **A740** (2004), 77.
13) Y. Kanada-En'yo, H. Horiuchi, and A. Ono, Phys. Rev. C **52** (1995), 628; Y. Kanada-En'yo and H. Horiuchi, Phys. Rev. C **52** (1995), 647.
14) Y. Kanada-En'yo, Phys. Rev. Lett. **81** (1998), 5291.
15) A. Doté, and H. Horiuchi, Prog. Theor. Phys. **103** (2000), 261.
16) M. Kimura and H. Horiuchi, Prog. Theor. Phys. **111** (2004), 841; nucl-th/040433.
17) Y. Taniguchi, M. Kimura and H. Horiuchi, Prog. Theor. Phys. **112** (2004), 475.
18) R. Tamagaki, Prog. Theor. Phys. **39** (1968), 91.
19) H. Furutani, H. Horiuchi and R. Tamagaki, Prog. Theor. Phys. **62** (1979), 981.
20) Y. Kanada-En'yo, M. Kimura and H. Horiuchi, Comptes Rendus Physique **4** (2003) 497.
21) R. B. Wiringa, V. G. J. Stoks and R. Schiavilla, Phys. Rev. C **51** (1995), 38.
22) A. Doté, Y. Kanada-En'yo and H. Horiuchi, Phys. Rev. C **56** (1997), 1844.
23) H. de Vries, C. W. de Jager and C. de Vries, Atomic Data and Nuclear Data Tables **36** (1987), 495.
24) K. Ikeda, Nucl. Phys. A **538** (1992), 355c.